We are IntechOpen, the world's leading publisher of Open Access books
Built by scientists, for scientists

6,900
Open access books available

185,000
International authors and editors

200M
Downloads

154
Countries delivered to

Our authors are among the

TOP 1%
most cited scientists

12.2%
Contributors from top 500 universities

CLARIVATE ANALYTICS
BOOK CITATION INDEX
INDEXED

WEB OF SCIENCE™

Selection of our books indexed in the Book Citation Index
in Web of Science™ Core Collection (BKCI)

Interested in publishing with us?
Contact book.department@intechopen.com

Numbers displayed above are based on latest data collected.
For more information visit www.intechopen.com

Application of PSO to design UPFC-based stabilizers

Ali T. Al-Awami[1], Mohammed A. Abido[1] and Youssef L. Abdel-Magid[2]
[1]King Fahd University of Petroleum & Minerals, [2]The Petroleum Institute
[1]Saudi Arabia, [2]United Arab Emirates

1. Introduction

Today, power demand grows rapidly and expansion in transmission and generation is restricted with the limited availability of resources and the strict environmental constraints. Consequently, power systems are today much more loaded than before. In addition, interconnection between remotely located power systems turned out to be a common practice. These give rise to low frequency oscillations in the range of 0.1-3.0 Hz. If not well damped, these oscillations may keep growing in magnitude until loss of synchronism results.

Power system stabilizers (PSSs) have been used in the last few decades to serve the purpose of enhancing power system damping to low frequency oscillations. PSSs have proved to be efficient in performing their assigned tasks. A wide spectrum of PSS tuning approaches has been proposed. These approaches have included pole placement (Chen & Hsu, 1987), damping torque concepts (Gibbard, 1988), H_∞ (Klein et al, 1995), variable structure (Samarasinghe & Pahalawaththa, 1997), and the different optimization and artificial intelligence techniques (Abdel-Magid et al, 1999; Abido, 2001; Abido & Abdel-Magid, 1997). However, PSS may adversely affect voltage profile and may not be able to suppress oscillations resulting from severe disturbances, such as three-phase faults at generator terminals (Mehran et al, 1992).

On the other hand, Flexible AC Transmission Systems (FACTS) have shown very promising results when used to improve power system steady-state performance. In addition, because of the extremely fast control action associated with FACTS-device operations, they have been very promising candidates for utilization in power system damping enhancement.

A unified power flow controller (UPFC) is the most promising device in the FACTS concept. It has the ability to adjust the three control parameters, i.e. the bus voltage, transmission line reactance, and phase angle between two buses. A major function of the UPFC is to redistribute power flow among transmission lines during steady state. During transients, it can be used to improve the damping of low frequency oscillations. To perform these tasks, the UPFC needs to be equipped with a power flow controller, a DC voltage regulator, and a supplementary damping controller.

Till now, not much research has been devoted to the analysis and control of UPFCs. Several trials have been reported in the literature to model a UPFC for steady-state and transient studies. Based on Nabavi-Iravani model (Nabavi-Niaki & Iravani, 1996), Wang developed a linearized UPFC model (Wang, 1999a & b) which has been incorporated into the Heffron-

Phillips model (Heffron & Phillips, 1952). Only a single operating point has been considered in the design process presented in (Wang, 1999a), which does not guarantee robust performance.

A number of control schemes have been suggested to perform the oscillation-damping task. Huang et al. (2000) attempted to design a conventional fixed-parameter lead-lag controller for a UPFC installed in the tie line of a two-area system to damp the interarea mode of oscillation. Mok et al. (2000) considered the design of an adaptive fuzzy logic controller for the same purpose. Dash et al. (2000) suggested the use of a radial basis function NN for a UPFC to enhance system damping performance. Robust control schemes, such as H∞ and singular value analysis, have also been explored (Vilathgamuwa et al, 2000; Pal, 2002). To avoid pole-zero cancellation associated with the H∞ approach, the structured singular value analysis have been utilized in (Seo et al, 2001) to select the parameters of the UPFC controller to have the robust stability against model uncertainties. However, the adaptive and robust control schemes proposed in (Mok et al, 2000; Dash et al, 2000; Vilathgamuwa et al, 2000; Pal, 2002; Seo et al, 2001) are still not widely implemented in power systems. In addition, the work cited proposed different techniques to design the damping controller without considering the power flow controller and the DC voltage regulator, or to design the three controllers sequentially, i.e. one at a time. To the best of the authors' knowledge, there has been no attempt till now to design the three controllers simultaneously.

1.1 Objectives

The objective of this chapter is to investigate the potential of particle swarm optimization as a tool in designing UPFC-based stabilizers to improve power system transient stability. To estimate the controllability of each of the UPFC control signals on the electromechanical modes, singular value decomposition is employed. The problem of designing all the UPFC-based stabilizers individually is formulated as an optimization problem. Particle swarm optimizer is utilized to search for the optimum stabilizer parameter settings that optimize a given objective function. Coordinated design of the different stabilizers is also carried out by finding the best parameter settings for more than one stabilizer at a given operating condition in a coordinated manner.

To further illustrate the potential of PSO in handling complex design problems, robust controller design using simultaneous stabilization is also explored. That is, to ensure the robustness of the proposed control schemes, the design procedure is repeated considering a wide range of operating conditions simultaneously in the design stage. To assess the effectiveness of the proposed designs, eigenvalue analysis as well as nonlinear time-domain simulations are carried out.

Two different objective functions will be considered. The first objective is eigenvalue-based while the other is time-domain-based. It will be shown that using a time-domain-based objective function has two advantages:

- Nonlinear models of the power system can be used in the design stage without the need for linearization.
- Coordinated designs of several controllers with different objectives can be achieved. (Abido et al, 2006b)

This chapter aims to demonstrate the potential of PSO in:

- Designing an individual UPFC-based stabilizer considering a single operating condition.

- Designing an individual UPFC-based stabilizer considering a wide range of operating conditions, i.e. robust control.
- Designing multiple UPFC-based stabilizers in a coordinated manner considering a wide range of operating conditions.
- Designing multiple UPFC-based stabilizers with different objectives in a coordinated manner using a time-domain objective function.

1.2 Definitions

At this point, it is worth emphasizing the meaning of the following terms:

Individual and coordinated designs: Individual design refers to the process of designing a single controller in the absence of any other controllers. Coordinated design, however, refers to the process of designing more than one controller concurrently so that coordination among the different controllers is achieved.

Single-point and robust tuning: Single-point tuning refers to the situation where a single operating condition is considered in the design stage. Robust tuning refers to the situation where multiple operating conditions are considered in the design stage to achieve robustness.

Simultaneous stabilization: Simultaneous stabilization refers to the technique used to design a controller taking into account several operating conditions. This technique guarantees the stability of the system at all the operating conditions considered in the design stage. The way simultaneous stabilization is implemented in this work, for the case of the eigenvalue-based objective function, is:

1. Declare a vector J
2. Pick an operating condition.
3. Linearize the system model around that operating condition.
4. Find the system complex eigenvalues and stack them in the vector J.
5. Repeat the same process (steps 2-4) until all operating conditions are covered. That is, vector J will contain all complex eigenvalues corresponding to all the considered operating conditions.
6. Search for the optimum controller's parameters that will push all those complex eigenvalues of J furthest to the left of the complex s-plane.

2. Problem Statement

Figure 1 shows a SMIB system equipped with a UPFC. The UPFC consists of an excitation transformer (ET), a boosting transformer (BT), two three-phase GTO based voltage source converters (VSCs), and a DC link capacitors. The four input control signals to the UPFC are m_E, m_B, δ_E, and δ_B, where

m_E is the excitation amplitude modulation ratio,

m_B is the boosting amplitude modulation ratio,

δ_E is the excitation phase angle, and

δ_B is the boosting phase angle.

2.1 Power System Nonlinear Model

By applying Park's transformation and neglecting the resistance and transients of the ET and BT transformers, the UPFC can be modeled as (Wang 1999a); Abido et al, 2006b):

$$: \quad \begin{bmatrix} v_{Etd} \\ v_{Etq} \end{bmatrix} = \begin{bmatrix} 0 & -x_E \\ x_E & 0 \end{bmatrix} \begin{bmatrix} i_{Ed} \\ i_{Eq} \end{bmatrix} + \begin{bmatrix} \dfrac{m_E \cos \delta_E v_{dc}}{2} \\ \dfrac{m_E \sin \delta_E v_{dc}}{2} \end{bmatrix} \tag{1}$$
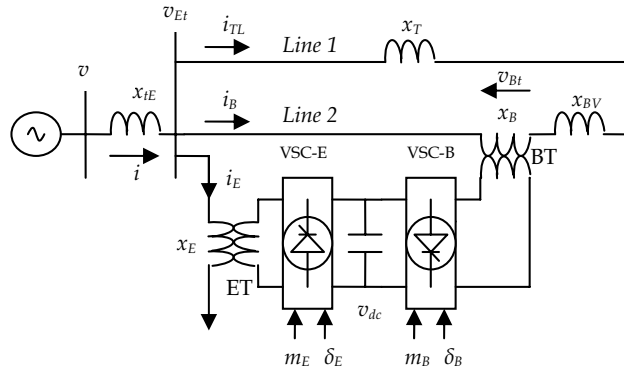
$$\begin{bmatrix} v_{Btd} \\ v_{Btq} \end{bmatrix} = \begin{bmatrix} 0 & -x_B \\ x_B & 0 \end{bmatrix} \begin{bmatrix} i_{Bd} \\ i_{Bq} \end{bmatrix} + \begin{bmatrix} \dfrac{m_B \cos \delta_B v_{dc}}{2} \\ \dfrac{m_B \sin \delta_B v_{dc}}{2} \end{bmatrix} \tag{2}$$

Figure 1. SMIB power system equipped with UPFC

$$\overset{\bullet}{v}_{dc} = \frac{3m_E}{4C_{dc}} \begin{bmatrix} \cos \delta_E & \sin \delta_E \end{bmatrix} \begin{bmatrix} i_{Ed} \\ i_{Eq} \end{bmatrix} + \frac{3m_B}{4C_{dc}} \begin{bmatrix} \cos \delta_B & \sin \delta_B \end{bmatrix} \begin{bmatrix} i_{Bd} \\ i_{Bq} \end{bmatrix} \tag{3}$$

where v_{Et}, i_E, v_{Bt}, and i_B are the excitation voltage, excitation current, boosting voltage, and boosting current, respectively; C_{dc} and v_{dc} are the DC link capacitance and voltage, respectively.

The ET, BT and line 2 currents can be stated as:

$$i_{TLd} = \frac{1}{x_T}(x_E i_{Ed} + \frac{m_E \sin \delta_E v_{dc}}{2} - v_b \cos \delta) \tag{4}$$

$$i_{TLq} = \frac{1}{x_T}(x_E i_{Eq} - \frac{m_E \cos \delta_E v_{dc}}{2} + v_b \sin \delta) \tag{5}$$

$$i_{Ed} = \frac{x_{BB}}{x_{d2}} E_q' + x_{d7} \frac{m_B \sin \delta_B v_{dc}}{2} + x_{d5} v_b \cos \delta + x_{d6} \frac{m_E \sin \delta_E v_{dc}}{2} \tag{6}$$

$$i_{Eq} = x_{q7} \frac{m_B \cos \delta_B v_{dc}}{2} + x_{q5} v_b \sin \delta + x_{q6} \frac{m_E \cos \delta_E v_{dc}}{2} \tag{7}$$

$$i_{Bd} = \frac{x_E}{x_{d2}} E_q' - \frac{x_{d1}}{x_{d2}} \frac{m_B \sin \delta_B v_{dc}}{2} + x_{d3} v_b \cos \delta + x_{d4} \frac{m_E \sin \delta_E v_{dc}}{2} \tag{8}$$

$$i_{Bd} = \frac{x_{q1}}{x_{q2}} \frac{m_B \cos \delta_B v_{dc}}{2} + x_{q3} v_b \sin \delta + x_{q4} \frac{m_E \cos \delta_E v_{dc}}{2} \tag{9}$$

where x_E and x_B are the ET and BT reactances, respectively; the reactances x_{qE}, x_{dE}, x_{BB}, x_{d1}-x_{d7}, and x_{q1}- x_{q7} are as shown in (Abido et al, 2006b).
The non-linear model of the SMIB system of Figure 1 is:

$$\dot{\delta} = \omega_b(\omega - 1) \tag{10}$$

$$\dot{\omega} = (P_m - P_e - D(\omega - 1))/M \tag{11}$$

$$\dot{E_q'} = (E_{fd} - (x_d - x_d')i_d - E_q')/T_{do}' \tag{12}$$

$$\dot{E_{fd}} = (K_A(V_{ref} - v + u_{PSS}) - E_{fd})/T_A \tag{13}$$

where $P_e = v_d i_d + v_q i_q$, $v = (v_d^2 + v_q^2)^{1/2}$, $v_d = x_q i_q$, $v_q = E_q' - x_d' i_d$, $i_d = i_{Ed} + i_{Bd}$, $i_q = i_{Eq} + i_{Bq}$

P_m and P_e are the input and output power, respectively; M and D the inertia constant and damping coefficient, respectively; ω_b the synchronous speed; δ and ω the rotor angle and speed, respectively; E_q', E'_{fd}, and v the generator internal, field and terminal voltages, respectively; T'_{do} the open circuit field time constant; x_d, x'_d, and x_q the d-axis reactance, d-axis transient reactance, and q-axis reactance, respectively; K_A and T_A the exciter gain and time constant, respectively; V_{ref} the reference voltage; and u_{PSS} the PSS control signal.

2.2 Power System Linearized Model
The non-linear dynamic equations can be linearized around a given operating point to have the linear model given by:

$$\dot{x} = Ax + Bu \tag{14}$$

where the state vector x, control vector u, and matrices A and B are

$$x = \begin{bmatrix} \Delta\delta & \Delta\omega & \Delta E_q' & \Delta E_{fd} & \Delta v_{dc} \end{bmatrix}^T \tag{15}$$

$$u = \begin{bmatrix} \Delta u_{pss} & \Delta m_E & \Delta \delta_E & \Delta m_b & \Delta \delta_b \end{bmatrix}^T \tag{16}$$

$$A = \begin{bmatrix} 0 & \omega_b & 0 & 0 & 0 \\ -\dfrac{K_1}{M} & -\dfrac{D}{M} & -\dfrac{K_2}{M} & 0 & -\dfrac{K_{pd}}{M} \\ -\dfrac{K_4}{T_{do}'} & 0 & -\dfrac{K_3}{T_{do}'} & \dfrac{1}{T_{do}'} & -\dfrac{K_{qd}}{T_{do}'} \\ -\dfrac{K_A K_5}{T_A} & 0 & -\dfrac{K_A K_6}{T_A} & -\dfrac{1}{T_A} & -\dfrac{K_A K_{vd}}{T_A} \\ K_7 & 0 & K_8 & 0 & -K_9 \end{bmatrix} \tag{17}$$

$$B = \begin{bmatrix} 0 & 0 & 0 & 0 & 0 \\ 0 & -\dfrac{K_{pe}}{M} & -\dfrac{K_{p\delta e}}{M} & -\dfrac{K_{pb}}{M} & -\dfrac{K_{p\delta b}}{M} \\ 0 & -\dfrac{K_{qe}}{T'_{do}} & \dfrac{K_{q\delta e}}{T'_{do}} & \dfrac{K_{qb}}{T'_{do}} & \dfrac{K_{q\delta b}}{T'_{do}} \\ \dfrac{K_A}{T_A} & -\dfrac{K_A K_{ve}}{T_A} & \dfrac{K_A K_{v\delta e}}{T_A} & \dfrac{K_A K_{vb}}{T_A} & \dfrac{K_A K_{v\delta b}}{T_A} \\ 0 & K_{ce} & K_{c\delta e} & K_{cb} & K_{c\delta b} \end{bmatrix} \tag{18}$$

where $K_1 - K_9$, K_{pu}, K_{qu}, and K_{vu} are linearization constants.

2.3 Structures of UPFC Controllers

The UPFC damping controllers are of the structure shown in Figure 2, where u can be m_E, δ_E, m_B, or δ_B.

In order to maintain the power balance between the series and shunt converters, a DC voltage regulator must be incorporated. The DC voltage is controlled through modulating the phase angle of the ET voltage, δ_E. In addition, to dispatch the power flow among transmission lines, a power flow controller is included. The power flow is controlled through modulation the amplitude of the BT voltage, m_B. Therefore, the δ_E and m_B damping controllers to be considered are those shown in Figure 3 and Figure 4, where the DC voltage regulator and the power flow controller are PI-controllers.

2.4 Objective Functions and Stabilizers' Design

To select the best stabilizer parameters that enhance most the power system transient performance, two objective functions are considered, one is eigenvalue-based and the other is time-domain-based. The eigenvalue-based objective function is:

$$J_e = \max[\sigma] \tag{19}$$

where σ is a vector of the real parts of all the complex eigenvalues (the damping factors) of the system at all loading conditions considered.
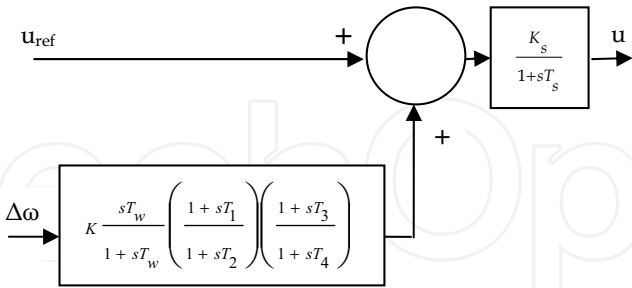

Figure 2. UPFC with lead-lag damping controllers

The objective function J_e identifies the maximum value of the damping factors, i.e. the real parts of the eigenvalues, among all the system complex modes of all loading conditions considered in the design process. Hence, the goal is to Minimize J_e to shift the poorly damped eigenvalues to the left in the s-plane improving the system response settling time and enhancing the system relative stability. It is worth emphasizing that by minimizing J_e,

all the operating conditions considered in the design stage are damped simultaneously. It is noteworthy that J_e is used to design the damping controllers only. That is, the UPFC DC voltage regulator and power flow controller must be designed beforehand.

In order to be able to design the damping controller, DC voltage regulator, and power flow controller in a coordinated manner, a time-domain-based objective function is used. This objective function is called the integral of time multiplied by absolute error (ITAE) and is defined as

$$J_t = \alpha \int t \,|\Delta\omega|\, dt + \beta \int t \,|\Delta P_{e2}|\, dt + \gamma \int t \,|\Delta V_{dc}|\; dt \qquad (20)$$

where $\Delta\omega$, ΔP_{e2}, and ΔV_{dc} are the deviations in system speed, real power flow of line 2, and DC voltage of the capacitor link, α, β, and γ are weighting factors.
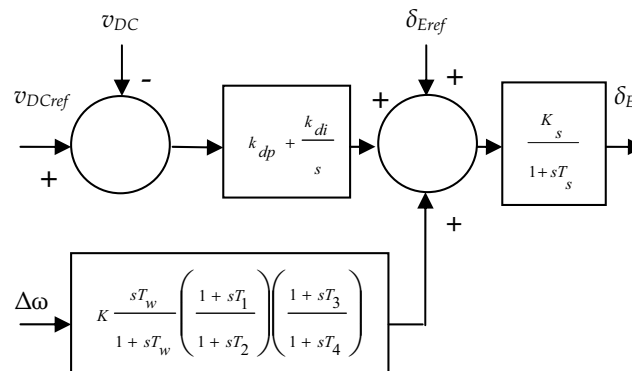

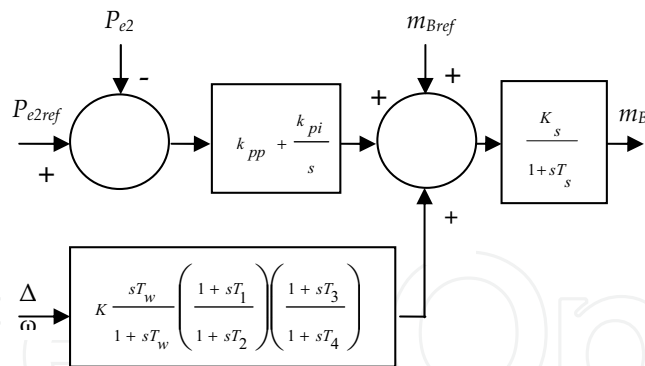Figure 3. UPFC with lead-lag damping controller and DC voltage regulator

Figure 4. UPFC with lead-lag damping controller and power flow controller

Hence, the design problem can be formulated as:

$$\text{minimize } J$$

Subject to

$$K_j^{\min} \leq K_j \leq K_j^{\max}$$
$$T_{ji}^{\min} \leq T_{ji} \leq T_{ji}^{\max}$$

where i = 1, 2, 3, or 4, and K_j and T_{ji} are the gain and time constants of the jth damping controllers.

The proposed approach employs PSO to search for the optimum parameter settings of the given controllers.

3. Controllability Measure

To measure the controllability of the EM mode by a given input (control signal), the singular value decomposition (SVD) is employed. The matrix B can be written as $B = [b_1\ b_2\ b_3\ b_4\ b_5]$ where b_i is a column vector corresponding to the ith input.

The minimum singular value, σ_{min}, of the matrix $[\lambda I\text{-}A\ b_i]$ indicates the capability of the ith input to control the mode associated with the eigenvalue λ. Actually, the higher the σ_{min}, the higher the controllability of this mode by the input considered. As such, the controllability of the EM mode can be examined with all inputs in order to identify the most effective one to control the mode. (Hamdan, 1999; Al-Awami et al, 2005)

4. Particle Swarm Optimization

Particle Swarm Optimization (PSO) was introduced first in (Kennedy & Eberhart, 1995). PSO approach features many advantages; it is simple, fast and can be coded in few lines. Also, its storage requirement is minimal.

Moreover, this approach is advantageous over evolutionary and genetic algorithms in many ways. First, PSO has memory. That is, every particle remembers its best solution (personal best – *pbest*) as well as the group best solution (global best – *gbest*). Another advantage of PSO is that the initial population of the PSO is maintained, and so there is no need for applying operators to the population, a process that is time- and memory-storage consuming. (Kennedy & Eberhart, 1995; Eberhart & Kennedy, 1995; Shi & Eberhart, 1998)

PSO starts with a population of random solutions "particles" in a D-dimension space. The ith particle is represented by $X_i=(x_{i1},\ x_{i2},\ \ldots,\ x_{iD})$. PSO consists of, at each step, changing the velocity of each particle toward its *pbest* and *gbest* according to equation (21). The velocity of particle i is represented as $V_i=(v_{i1},\ v_{i2},\ \ldots,\ v_{iD})$. The position of the ith particle is then updated according to equation (22) (Kennedy & Eberhart, 1995; Eberhart & Kennedy, 1995; Shi & Eberhart, 1998).

$$v_{id} = wv_{id} + c_1 r_1 (p_{id} - x_{id}) + c_2 r_2 (p_{gd} - x_{gd}) \qquad (21)$$

$$x_{id} = x_{id} + v_{id} \qquad (22)$$

where, $p_{id} = pbest$ and $p_{gd} = gbest$

An excellent simplified description of the PSO algorithm can be found in (Abido, 2001).

Figure 5 shows a flow chart of the PSO algorithm that is adopted for this specific problem. It is described as follows:

Step 1: Define the problem space and set the boundaries, i.e. the acceptable limits of the controller parameters.

Step 2: Initialize an array of particles with random positions and their associated velocities inside the problem space. These particle positions represent the initial set of solutions.
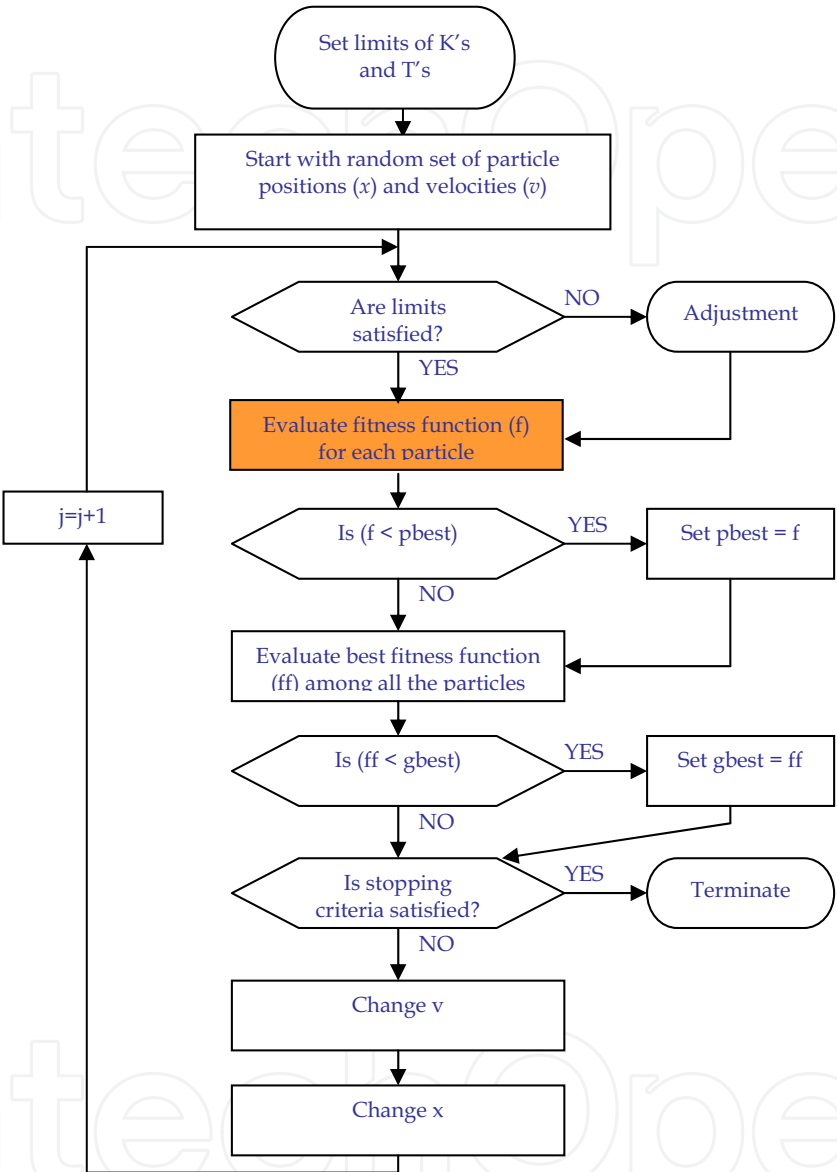
Figure 5. Particle Swarm Optimization algorithm

Step 3: Check if the current position is inside the problem space or not. If not, adjust the positions so as to be inside the problem space.

Step 4: Evaluate the fitness value of each particle.

Step 5: Compare the current fitness value with the particles' previous best value ($pbest_i$). If the current fitness value is better, then assign the current fitness value to $pbest_i$ and assign the current coordinates to $pbestx_i$ coordinates.

Step 6: Determine the current global minimum among particle's best position.

Step 7: If the current global minimum is better than *gbest*, then assign the current global minimum to *gbest* and assign the current coordinates to *gbestx* coordinates.
Step 8: Change the velocities according to (21).
Step 9: Move each particle to the new position according to (22) and return to Step 3.
Step 10: Repeat **Step 3- Step 9** until a stopping criteria is satisfied.
To adopt the PSO algorithm so that simultaneous stabilization is achieved, i.e. several operating points are considered simultaneously, the fitness function evaluation process contains an inner loop, see Figure 6. That is, for every operating point i, the objective J_i is computed. Then, $J = \max(J_1, J_2, ..., J_{N_{op}})$, where N_{op} is the number of operating points considered, is evaluated. (Al-Awami et al, 2006a; Al-Awami et al, 2007; Abido et al, 2006b)
The proposed PSO–based approach was implemented using a MATLAB library built by the authors. In all implementations, the inertia weight, w, is linearly decreasing from 0.9 to 0.4, c_1 and c_2 are selected as 2, and the maximum number of iterations is 400.

5. Simulation Results

5.1 Electromechanical Mode Controllability Measure
Singular value decomposition (SVD) is employed to measure the controllability of the electromechanical mode (EM) from each of the four UPFC inputs: m_E, δ_E, m_B, and δ_B. For comparison, the power system stabilizer input, u_{pss}, is also included. The minimum singular value, σ_{min}, is estimated over a wide range of operating conditions. For SVD analysis, P_e ranges from 0.05 to 1.4 pu and Q_e= [-0.4, 0, 0.4]. At each loading condition, the system model is linearized, the EM mode is identified, and the SVD-based controllability measure is implemented. (Al-Awami et al, 2007)
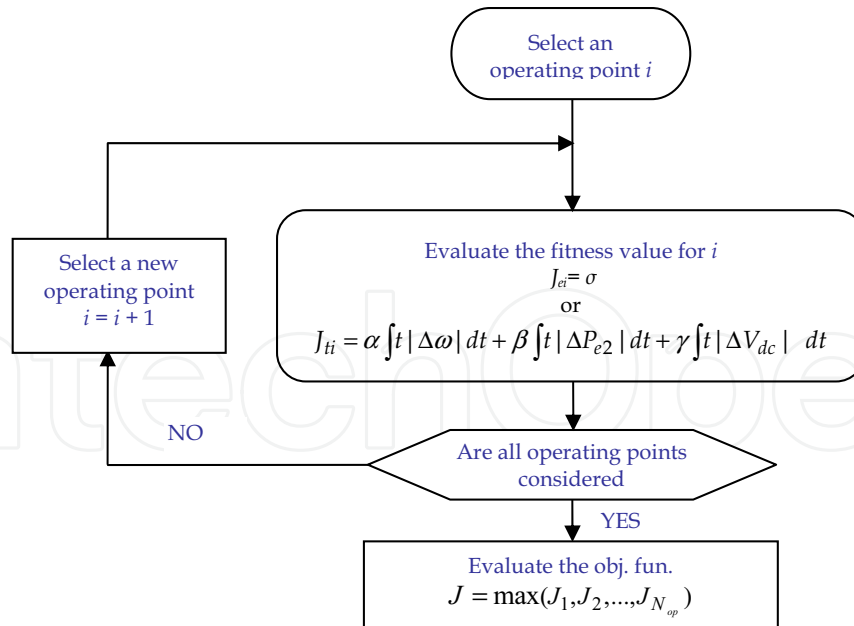

Figure 6. Particle Swarm Optimization adopted for simultaneous stabilization

For comparison purposes, the minimum singular value for all inputs at Qe = - 0.4, 0.0 and 0.4 pu is shown in Figures 7, 8, and 9, respectively. From these figures, the following can be noticed:

- EM mode controllability via δ_E is always higher than that of any other input.
- The capabilities of δ_E and m_B to control the EM mode is higher than that of PSS.
- The EM mode is more controllable with PSS than with either m_E or δ_B.
- All control signals except m_B at Q_e = 0 and δ_E suffer from low controllability to EM mode at low loading conditions.

5.2 Design and Analysis Using Eigenvalue-based Objective Function J_e

In this section, stabilizer design is carried out using the eigenvalue-based objective function, J_e, given by (19). Both single-point tuning and robust tuning using simultaneous stabilization are presented. A coordinated design of stabilizers is also demonstrated. The system used is that shown in Figure 1 and the system data used is given in the Appendix. (Al-Awami et al, 2007; Al-Awami et al, 2005; Al-Awami et al, 2006)

To assess the effectiveness of the proposed controllers, four different loading conditions are considered for eigenvalue analysis, see Table 1.

Moreover, the nominal and light loading conditions with 6-cycle three-phase fault disturbances are considered for nonlinear time-domain simulations.

Loading Condition	(P_e, Q_e) pu
Nominal	(1.0, 0.015)
Light	(0.3, 0.015)
Heavy	(1.1, 0.400)
Leading Pf	(0.7, -0.30)

Table 1. Loading conditions

5.2.1 Single-point Tuning Using J_e

The PSS, m_E-, δ_E-, m_B-, and δ_B-based stabilizers are designed individually considering the nominal loading condition. PSO is used to search for the optimum parameter settings of each controller individually so as to minimize the maximum damping factor of all the system complex eigenvalues at nominal loading condition. The final settings of the optimized parameters for the proposed stabilizers and the minimum damping factors achieved are given in Table 2.

The system electromechanical mode without and with the proposed stabilizers at the four operating points, nominal, light, heavy, and leading Pf, are given in Table 3. Table 3 clearly demonstrate the effectiveness of the δ_E- and m_B-based stabilizers in enhancing system stability. Again, It can be observed that, in most cases, the EM mode is either unstable or poorly damped when driven by m_E- or δ_B-based stabilizers. This conclusion is in line with those already drawn from SVD analysis. Because of their poor performance, the m_E- and δ_B-based stabilizers will be excluded from the analysis hereafter.

The system behaviour due to the utilization of the proposed controllers under transient conditions has been tested by applying a 6-cycle 3-phase fault at the infinite bus at t = 1s. The system response at nominal loading is shown in Figures 10 and 11, and the response at light loading is shown in Figures 12 and 13. From these figures, the following can be observed:

- The three stabilizers designed with the proposed PSO-based technique effectively improve the stability of the power system under study.

- As expected from SVD analysis, the δ_E-based stabilizer is robust to operating point variations.
- Both UPFC-based stabilizer outperform the PSS in terms of their effect on voltage profile.
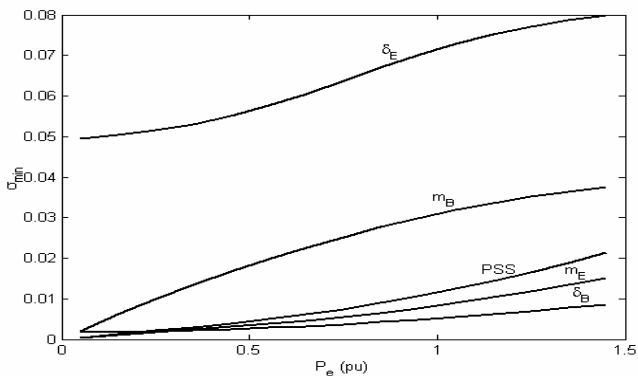

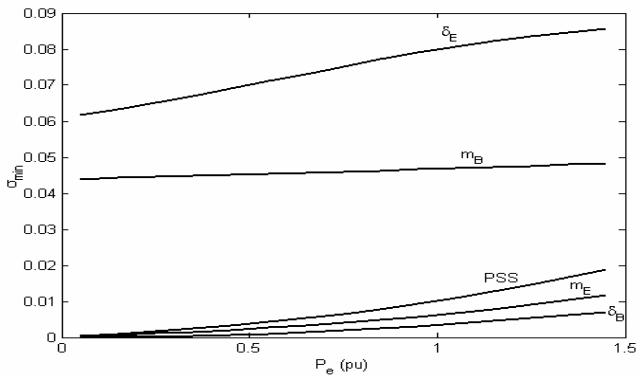Figure 7. Minimum singular value with all stabilizers at $Q_e = -0.4$

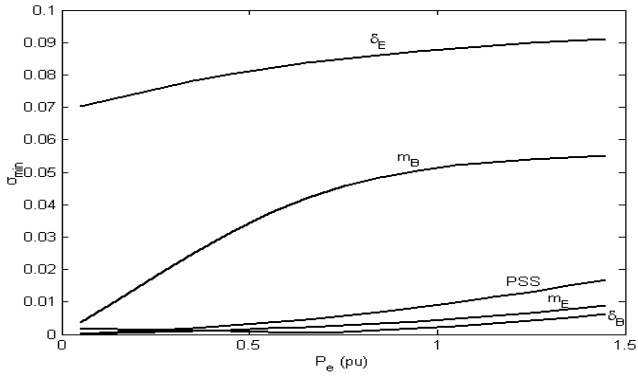Figure 8. Minimum singular value with all stabilizers at $Q_e = 0.0$

Figure 9. Minimum singular value with all stabilizers at $Q_e = 0.4$

	PSS	m_E	δ_E	m_B	δ_B
K	29.26	-29.83	-100.00	100.00	-72.89
T_1	2.92	0.25	5.00	0.11	2.02
T_2	1.19	2.46	1.08	0.01	0.13
T_3	0.13	2.95	0.06	2.18	2.94
T_4	0.01	0.01	1.44	2.35	2.42
J_e	-5.44	-1.69	-4.63	-4.15	-1.39

Table 2. Optimal parameter settings with J_e, single-point tuning, individual design

	No Control	PSS	m_E	δ_E	m_B	δ_B
N	$1.50 \pm 5.33i$	$-5.44 \pm 0.18i$	$-1.69 \pm 7.62i$	$-4.62 \pm 5.88i$	$-4.15 \pm 6.06i$	$-1.39 \pm 6.02i$
L	$1.39 \pm 5.08i$	$-1.10 \pm 4.67i$	$0.90 \pm 5.37i$	$-3.17 \pm 5.88i$	$-3.24 \pm 6.88i$	$1.30 \pm 5.12i$
H	$1.41 \pm 5.00i$	$-1.71 \pm 2.00i$	$0.08 \pm 7.05i$	$-1.81 \pm 1.74i$	$-4.62 \pm 3.75i$	$-1.79 \pm 5.48i$
L_{pf}	$1.45 \pm 5.35i$	$-5.70 \pm 16.79i$	$-0.81 \pm 6.34i$	$-1.97 \pm 5.48i$	$-1.37 \pm 6.07i$	$-0.26 \pm 5.58i$

Table 3. System electromechanical modes at all loading conditions with no parameter uncertainties with J_e settings, single-point tuning, individual design (N: Nominal, L: Light, H: Heavy, L_{pf}: Leading power factor)

5.2.2 Robust Tuning with Simultaneous Stabilization Using J_e

In this situation, the objective is to design robust stabilizers to ensure their effectiveness over a wide range of operating conditions. Both individual and coordinated designs are considered. The design process takes into account several loading conditions including nominal, light, heavy, and leading Pf conditions. These conditions are considered without and with system parameter uncertainties, such as machine inertia, line impedance, and field time constant. The total number of 16 operating conditions is considered during the design process as given in Table 4.
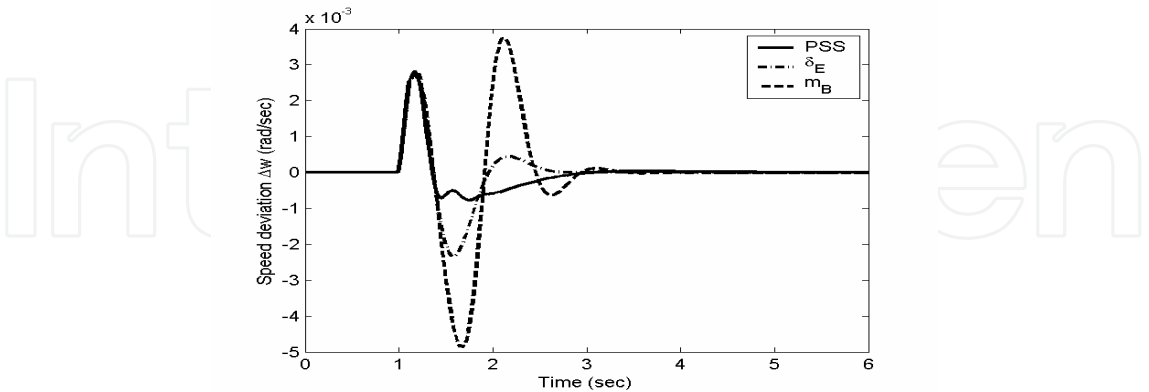

Figure 10. Speed response for 6-cycle fault with nominal loading, J_e settings, single-point tuning, individual design
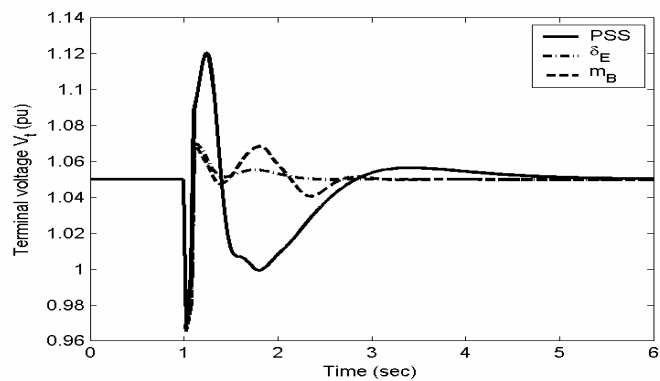
Figure 11. Terminal voltage response for 6-cycle fault with nominal loading, J_e settings, single-point tuning, individual design
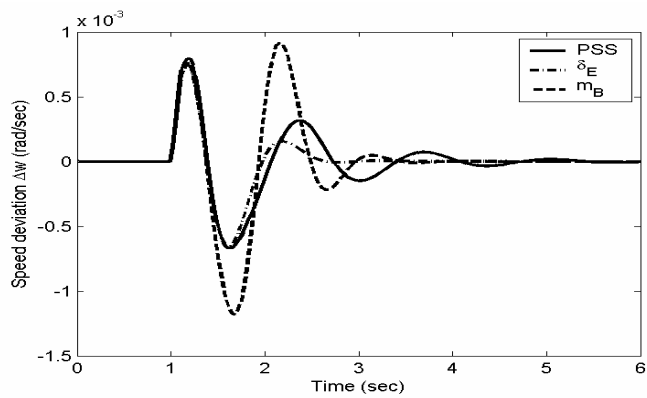

Figure 12. Speed response for 6-cycle fault with light loading, J_e settings, single-point tuning, individual design
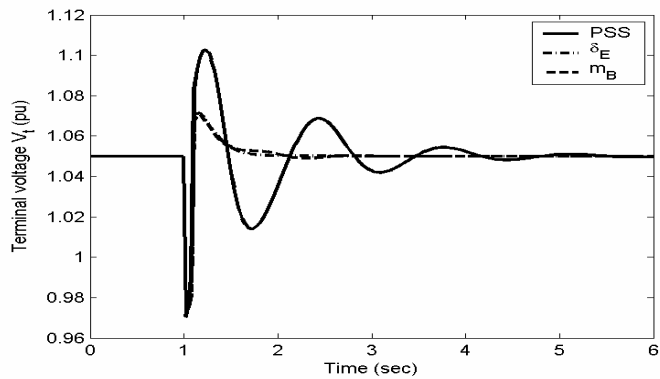

Figure 13. Terminal voltage response for 6-cycle fault with light loading, J_e settings, single-point tuning, individual design

Loading Condition	(P_e, Q_e) pu	Parameter Uncertainties
N	(1.0, 0.015)	No parameter uncertainties
L	(0.3, 0.100)	30% increase of line reactance X_{BV}
H	(1.1, 0.100)	25% decrease of machine inertia M
L_{pf}	(0.7, -0.30)	30% decrease of field time constant T'_{do}

Table 4. Loading conditions and parameter uncertainties considered in the design stage

Table 5 lists the open-loop eigenvalues associated with the electromechanical modes of all the 16 operating points considered in the robust design process, respectively. It is evident that all these modes are unstable.

In the individual design, the PSS, δ_E-, and m_B--based stabilizers are designed individually considering all the operating points mentioned above. PSO is used to optimize the parameters of each controller that minimize the maximum damping factor of all the complex eigenvalues associated with the 16 operating points simultaneously. The final settings of the optimized parameters for the proposed stabilizers and the minimum damping factors achieved are given in Table 6.

The system electromechanical mode without and with the proposed stabilizers at the four operating points, nominal, light, heavy, and leading Pf, are given in Table 7. Table 7 clearly demonstrate the effectiveness of the proposed stabilizers in enhancing system stability. Comparing Table 7 with Table 3, the effectiveness of robust tuning with simultaneous stabilization can be observed. For example, the maximum damping factor of the system electromechanical modes using single-point tuning for PSS is -1.10. However, the maximum damping factor using robust tuning with simultaneous stabilization is -2.58.

The system behaviour due to the utilization of the proposed stabilizers under transient conditions has been tested by applying a 6-cycle 3-phase fault at the infinite bus at $t = 1$s. The system response at nominal loading is shown in Figures 14 and 15, and the response at light loading is shown in Figures 16 and 17. These simulation results prove the effectiveness of the proposed technique in designing robust stabilizers. It can be observed by comparing Figure 12 with Figure 16 that including the light loading condition in the robust tuning technique helped improve PSS response to transients in the system. In addition, it can be readily seed again that both UPFC-based stabilizer outperform the PSS in terms of their effect on voltage profile.

	No parameter uncertainties	30% increase of line reactance X	25% decrease of machine inertia M	30% decrease of field time constant T'_{do}
N	$1.50 \pm 5.33i$	$1.41 \pm 4.99i$	$1.80 \pm 5.94i$	$1.5034 \pm 5.40i$
L	$1.39 \pm 5.08i$	$1.32 \pm 4.74i$	$1.67 \pm 5.66i$	$1.3951 \pm 5.09i$
H	$1.41 \pm 5.00i$	$1.25 \pm 4.52i$	$1.70 \pm 5.57i$	$1.4038 \pm 5.08i$
L_{pf}	$1.45 \pm 5.35i$	$1.40 \pm 5.08i$	$1.74 \pm 5.97i$	$1.4498 \pm 5.39i$

Table 5. Open-loop eigenvalues associated with the EM modes of all the 16 points considered in the robust design process

Although the controllability measure analysis based on the singular value decomposition and the nonlinear time-domain simulation show the relative robustness of the δ_E-based

stabilizer in damping the EM mode oscillation, there is still room for more improvement through coordination with the m_B-based stabilizer. In the following, the coordinated design of δ_E- and m_B-based stabilizers is considered at all the 16 operating points described earlier. PSO is used to simultaneously search for the optimum parameter settings of both controllers that minimize the maximum damping factor of all the system complex eigenvalues at all the 16 operating points concurrently. The final settings of the optimized parameters for the proposed stabilizers are given in Table 8.

	PSS	δ_E	m_B
K	95.58	-100.00	96.8
T_1	4.34	5.00	4.99
T_2	0.01	1.03	2.57
T_3	0.07	0.06	0.12
T_4	3.51	1.54	0.01
J_e	-1.95	-1.77	-3.54

Table 6. Optimal parameter settings with J_e, multiple-point tuning, individual design

	No Control	PSS	δ_E	m_B
N	$1.50 \pm 5.33i$	$-2.58 \pm 17.5i$	$-3.52 \pm 5.32i$	$-3.91 \pm 12.7i$
L	$1.39 \pm 5.08i$	$-3.91 \pm 3.62i$	$-2.93 \pm 5.65i$	$-3.71 \pm 12.1i$
H	$1.41 \pm 5.00i$	$-2.80 \pm 17.0i$	$-1.92 \pm 1.76i$	$-3.56 \pm 13.1i$
L_{pf}	$1.45 \pm 5.35i$	$-2.72 \pm 16.2i$	$-1.82 \pm 5.47i$	$-3.53 \pm 2.61i$

Table 7. System electromechanical modes at all loading conditions with no parameter uncertainties with J_e settings, robust tuning, individual design
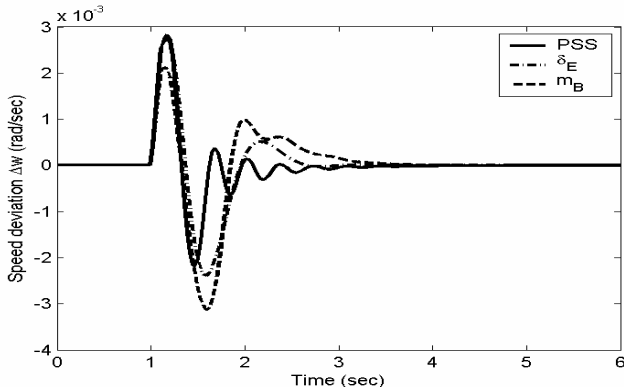

Figure 14. Speed response for 6-cycle fault with nominal loading, J_e settings, robust tuning, individual design

The system electromechanical modes without and with the proposed δ_E- and m_B-based controllers when applied individually and through coordinated design at the four loading conditions; nominal, light, heavy, and leading Pf, are given in Table 9. It is evident that the damping factor of the EM mode is greatly enhanced using the proposed coordinated stabilizers design.
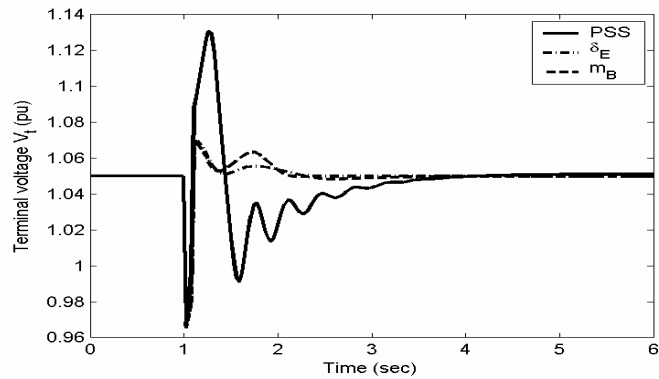
Figure 15. Terminal voltage response for 6-cycle fault with nominal loading, J_e settings, robust tuning, individual design
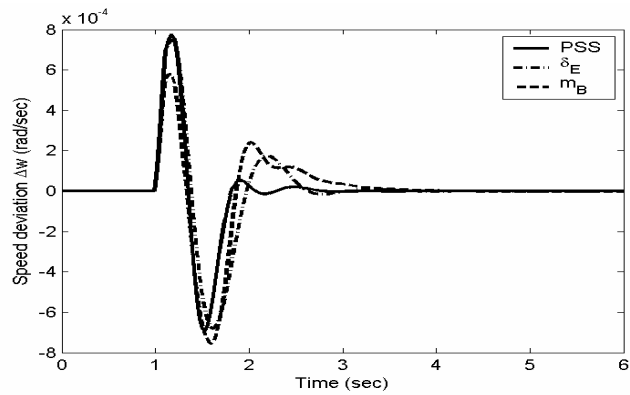

Figure 16. Speed response for 6-cycle fault with light loading, J_e settings, robust tuning, individual design
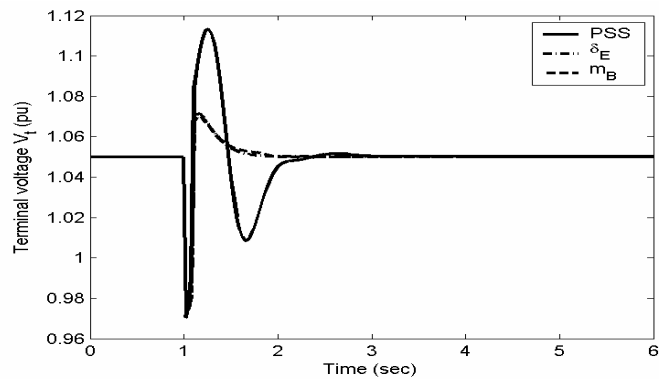

Figure 17. Terminal voltage response for 6-cycle fault with light loading, J_e settings, robust tuning, individual design

Moreover, the nonlinear time-domain simulations are carried out at the nominal and light loading conditions specified previously. The speed deviations, DC voltage, electrical power, and δ_E and m_B control signals for a 6-cycle three-phase fault at nominal loading conditions are shown in Figures 18-22, respectively. The simulation results indicate a clear enhancement of the proposed coordinated δ_E-m_B design over both individual designs. This enhancement can be easily recognized from the sound reduction in overshoot and settling time of the speed, electrical power and DC voltage responses as well as the reduction in the control efforts of the coordinated design as compared with the control efforts of the two individual designs. Similar conclusions can be drawn from light loading results. Due to limitation in space, only speed deviations at light loading conditions are shown, see Figure 23. It is noteworthy that using coordination, the problem of low effectiveness of the m_B-based stabilizer individual designs at light loading level has been solved.

	Individual		Coordinated	
	δ_E	m_B	δ_E	m_B
K	-100.00	96.8	-66.18	100.00
T_1	5.00	4.99	1.53	5.00
T_2	1.03	2.57	1.61	3.09
T_3	0.06	0.12	4.42	5.00
T_4	1.54	0.01	3.95	3.32

Table 8. Optimal parameter settings with J_e, multiple-point tuning, coordinated design

Loading	δ_E	m_B	δ_E & m_B
N	$-3.52 \pm 5.32i$	$-3.91 \pm 12.72i$	$-7.51 \pm 10.64i$
L	$-2.93 \pm 5.65i$	$-3.71 \pm 12.19i$	$-5.81 \pm 11.04i$
H	$-1.92 \pm 1.76i$	$-3.56 \pm 13.12i$	$-7.21 \pm 11.65i$
L_{pf}	$-1.82 \pm 5.47i$	$-3.53 \pm 2.61i$	$-5.86 \pm 6.46i$

Table 9 System eigenvalues with all the stabilizers at different loading conditions

5.3 Coordinated Design of Damping Stabilizers and Internal Controllers Using Time-domain-based Objective Function J_t

In this section, stabilizer design is carried out using the time-domain-based objective function, J_t, given by (20). Using J_t, the need for linearizing the nonlinear power system model is eliminated. That is, the nature of the objective function makes it suitable for both linear and nonlinear systems (Al-Awami et al, 2006b; Abido et al, 2006b). Moreover, it is possible to design several controllers with different objectives in a coordinated manner (Abido et al, 2006b). As will be shown, using the time-domain-based objective function, it is possible to design the UPFC damping controller, DC voltage regulator, and power flow controller, each of which has a different objective, in a coordinated manner. In this section, a coordinated design of UPFC damping stabilizers and internal controllers at nominal loading conditions is demonstrated. The effectiveness of the proposed controllers in damping low frequency oscillations is verified through eigenvalue analysis and non-linear time simulation. A comparison with a sequential design of the controllers under study is also included. The system used is that shown in Figure 1 and the system data used is given in the Appendix. (Abido et al, 2006b)
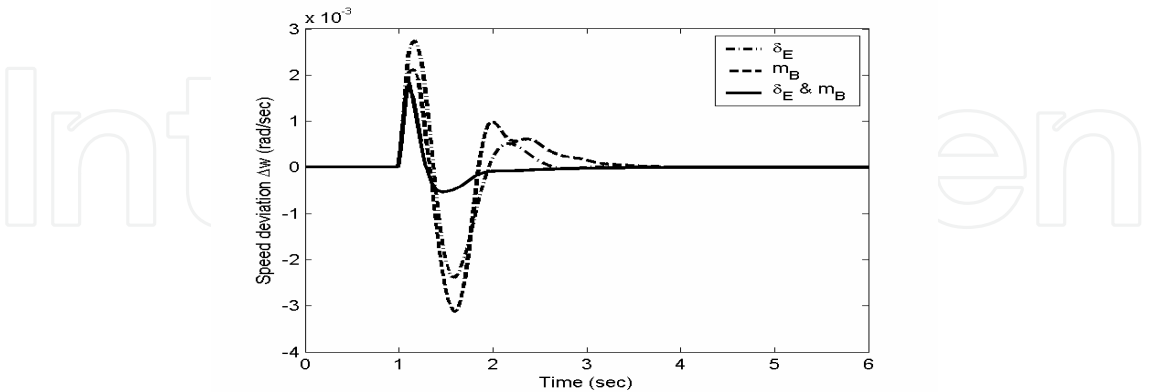
Figure 18. Speed response for 6-cycle fault with nominal loading, J_t settings, robust tuning, coordinated design
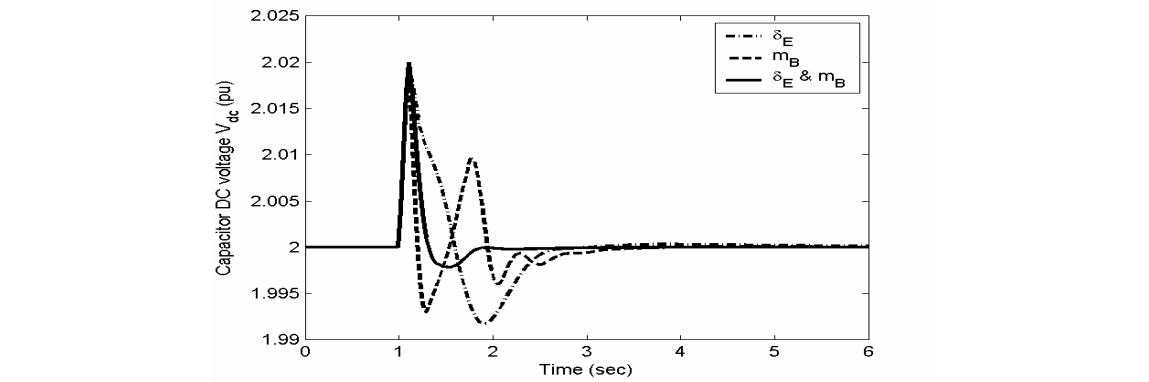

Figure 19. UPFC DC voltage response for 6-cycle fault with nominal loading, J_t settings, robust tuning, coordinated design
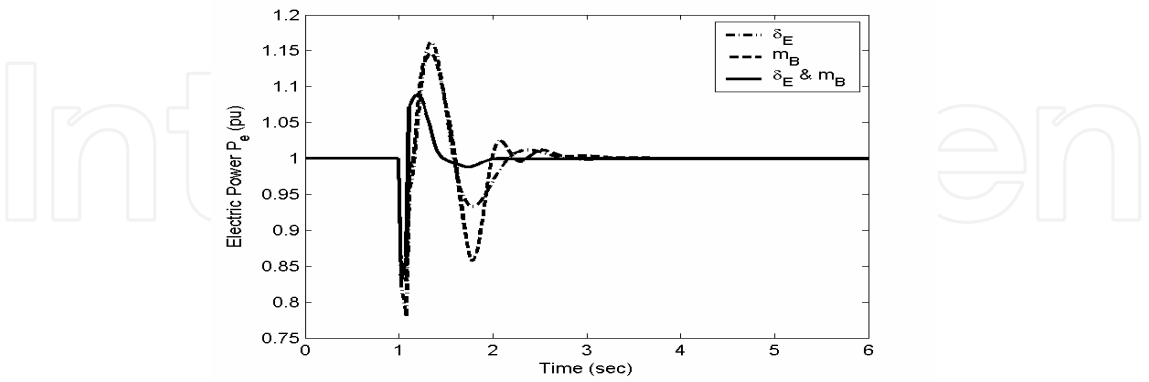

Figure 20. Electrical Power response for 6-cycle fault with nominal loading, J_t settings, robust tuning, coordinated design
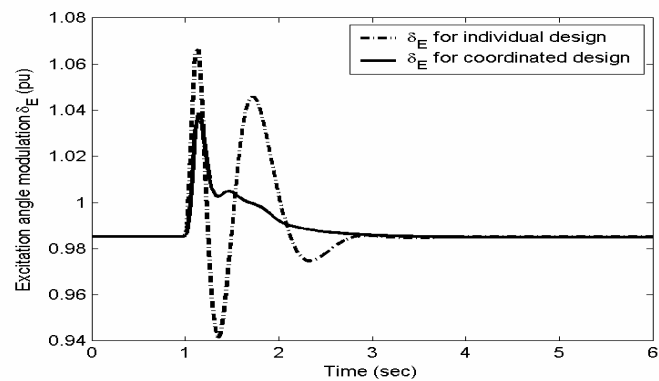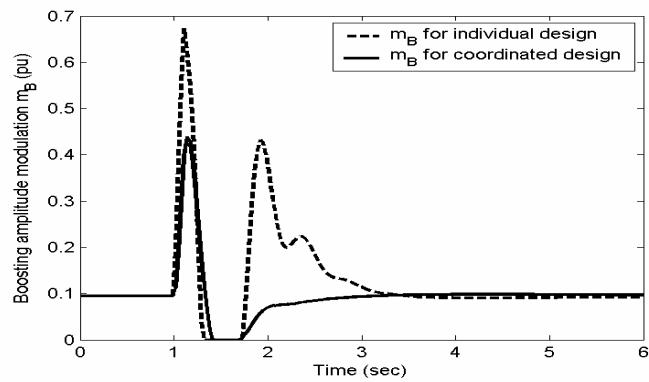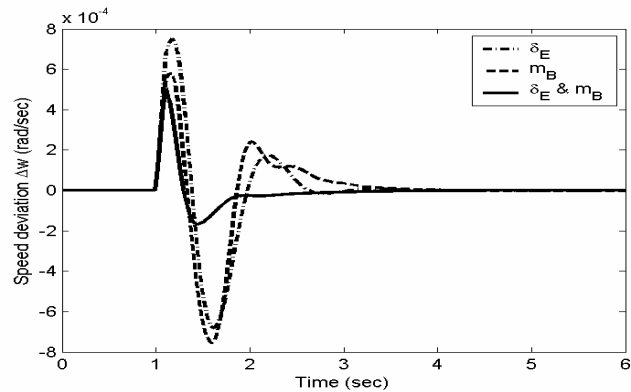
Figure 21. δ_E control signal response for 6-cycle fault with nominal loading, J_t settings, robust tuning, coordinated design

Figure 22. m_B control signal response for 6-cycle fault with nominal loading, J_t settings, robust tuning, coordinated design

Figure 23. Speed signal response for 6-cycle fault with light loading, J_t settings, robust tuning, coordinated design

5.3.1 Sequential Controller Design

In this stage, the three controllers are designed sequentially (Abido et al, 2006b). That is, (1) the DC voltage regulator (VR) is designed first, then (2) the power flow controller (PFC) is designed in the presence of the regulator, and finally (3) the damping controllers (DC) are designed, one at a time, in the presence of the other two controllers (VR and PFC). In each step, PSO has been used to find the optimum parameters of each controller that optimize the objective function defined by (20). A nominal loading condition has been considered in the design stage, see Table 10.

Since each of the three controllers has a different function, the objective function weights and the disturbances used in the design stage are different. Table 11 shows the details of each step in the sequential design. Step (1) resulted in the following optimum parameters for the DC voltage regulator: k_{dp} = – 4.56, k_{di} = – 19.98. Step (2) resulted in the following optimum parameters for the power flow controller: k_{pp} = 0.0005, k_{pi} = – 0.0047. The final settings of the optimized parameters for the proposed damping controllers are given in Table 12.

To test the performance of these stabilizers, eigenvalue analysis and nonlinear time-domain simulations are carried out. The system data is given in the Appendix The system EM modes and their corresponding damping ratios with the PSS and UPFC-based controllers when tested at nominal loading are given in Table 13. Moreover, the speed deviations for a 6-cycle three-phase fault at nominal loading conditions are shown in Figure 24. It is evident that the sequential designs give rise to poorly damped or even unstable responses.

Loading Condition	P_e (pu)	Q_e (pu)
Nominal	1.000	0.015
Light	0.300	0.100

Table 10. Loading Conditions

Controller	Weights of J			Disturbance
	α	β	γ	
VR	0	0	1	step change in V_{DCref}
PFC	0	1	0	step change in P_{e2ref}
DC	1	0	0	Impulse change in P_m

Table 11. Objective Function Weights and Disturbances Used in Steps (1)-(3) for the Sequential Design

	δ_E	m_B	PSS
K	83.94	92.31	71.37
T_1	1.18	0.40	0.27
T_2	1.01	0.63	0.69
T_3	1.50	1.49	0.34
T_4	0.57	0.72	0.05
J	36.21	139.88	0.29

Table 12. The Optimal Parameter Settings of the Individual Controllers – Sequential Design

	δ_E	m_B	PSS
EM	1.30 ± 3.10i	1.79 ± 7.39i	-0.80 ± 5.04i
ζ	-0.39	-0.24	0.16

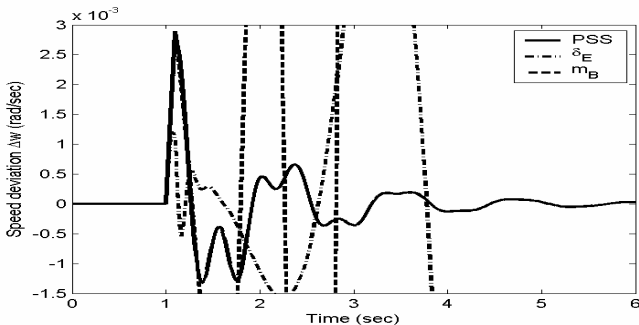Table 13. System Eigenvalues of the Individual Controllers at Nominal Loading – Sequential Design

Figure 24. Speed response for a 6-cycle fault with nominal loading – sequential design

5.3.2 Coordinated Controller Design

In this stage, the three controllers are designed in a coordinated manner (Abido et al, 2006b). That is, PSO is used to concurrently find the optimum parameters of the VR, PFC, and DC minimizing the error objective function defined in (20). In order to end up with the optimum controllers, the objective function weights and the disturbances have to be selected carefully. Table 14 shows the objective function weights used in every case. In all cases, the following two disturbances have been used:

1. An impulse change in P_m
2. A step change in P_{e2ref}.

The final settings of the optimized parameters for the proposed controllers are given in Table 15.

To test the performance of the proposed stabilizers, eigenvalue analysis and nonlinear time-domain simulations are carried out.

The system EM modes and their corresponding damping ratios with the proposed PSS and UPFC-based controllers when tested at nominal and light loading conditions are given in Table 16. It is evident that system stability is greatly enhanced by the proposed coordinated designs.

Damping Controller	Weights of J		
	α	β	γ
δ_E	100	1	30
m_B	120	1	10
PSS	100	1	10

Table 14. Objective Function Weights and Disturbances Used in the Simultaneous Design

	δ_E	m_B	PSS
K	100.00	100.00	1.64
T_1	1.28	1.50	0.62
T_2	0.76	0.49	0.17
T_3	0.05	1.50	1.01
T_4	0.57	0.49	0.05
k_{pp}	0.51	-13.21	-19.93
k_{pi}	-0.92	-14.60	-17.44
k_{dp}	-7.69	-20.00	-13.77
k_{di}	-2.19	-15.46	-5.41
J	124.9	35.0	27.0

Table 15. The Optimal Parameter Settings of the Individual Controllers – Simultaneous Design

		δ_E	m_B	PSS
N	EM	-2.15 ± 6.97i	-2.37 ± 6.49i	-1.97 ± 5.25i
	ζ	0.30	0.34	0.35
L	EM	-2.18 ± 6.59i	-2.44 ± 6.30i	-1.80 ± 8.72i
	ζ	0.31	0.36	0.20

Table 16. System Eigenvalues of the Individual Controllers at Nominal (N) and Light (L) Loading – Simultaneous Design

Moreover, the nonlinear time-domain simulations are carried out at nominal and light loading conditions. The deviations in speed, power flow of line 2, and DC voltage for a 6-cycle three-phase fault at nominal loading condition are shown in Figures 25-27, respectively. From these figures, it is observed that:

- The proposed coordinated designs give rise to superior responses.
- After the fault, the three signals shown in Figures 25-27 have settled with no steady-state error, excellent settling time, and reasonably good overshoot.
- The δ_E-based controller outperforms the m_B-based controller and PSS, especially in terms of overshoot.
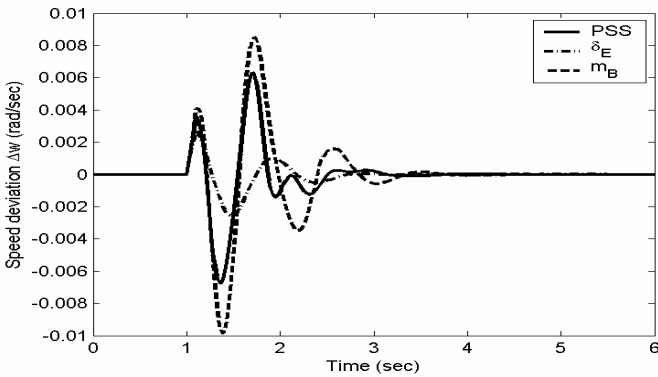
Figure 25. Speed response for a 6-cycle fault with nominal loading – Coordinated design
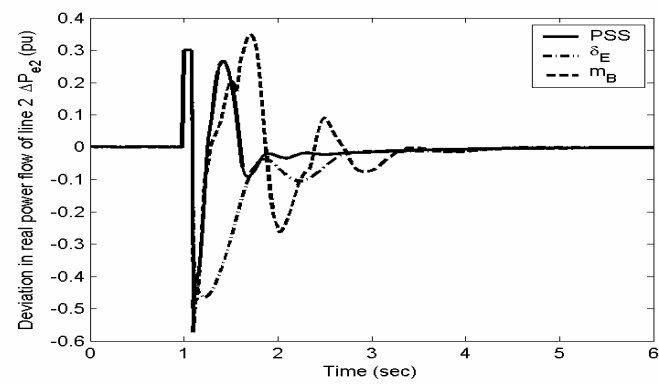
Figure 26. Power flow response of line 2 for a 6-cycle fault with nominal loading –
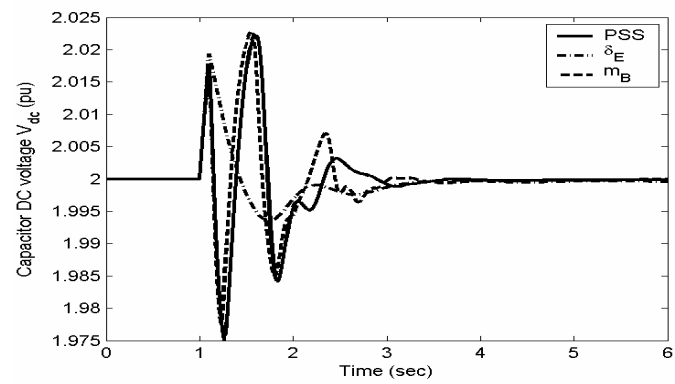Coordinated design

Figure 27. DC voltage response for a 6-cycle fault with nominal loading – Coordinated
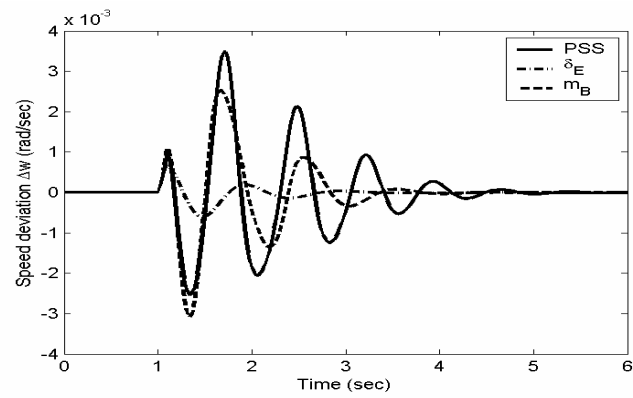design

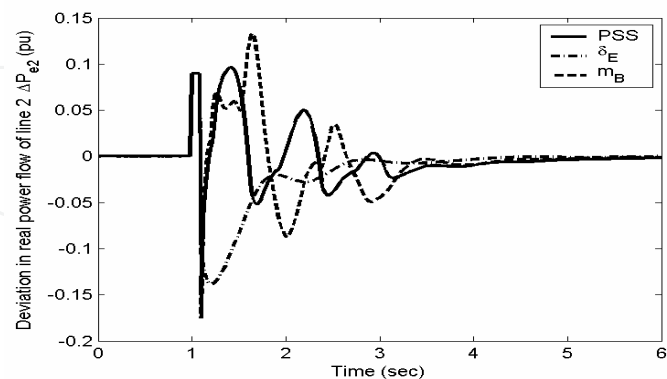Figure 28. Speed response for a 6-cycle fault with light loading – coordinated design

Figure 29. Power flow response of line 2 for a 6-cycle fault with light loading – simultaneous design
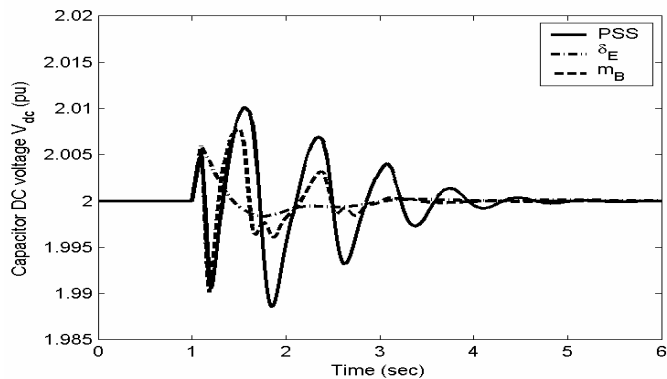

Figure 30. DC voltage response for a 6-cycle fault with light loading – simultaneous design

In addition, the deviations in torque angle, power flow of line 2, and DC voltage for a 6-cycle three-phase fault at light loading conditions are shown in Figures 28-30, respectively. From these figures it can be concluded that the δ_E-based controller is the most effective controller in terms of overshoot, settling time, and steady-state error. This shows that the performance of δ_E-based controller is almost unaffected with the loading level. The performance of m_B-based controller and PSS, however, is degraded at this loading condition.

6. Conclusion

In this work, the problem of enhancing the power system dynamic stability through individual and coordinated design of UPFC-based damping stabilizers has been investigated. The controllability of the electromechanical mode over a wide range of operating conditions by a given control input has been measured using a singular value decomposition-based approach. Such a study is very important as it laid the foundations of the requirements of the coordinated design problem. The stabilizer design problem has been formulated as an optimization problem with an eigenvalue-based as well as a time domain-

based objective functions, which was then solved by particle swarm optimization. The use of the first objective function results in placing the electromechanical modes of oscillations furthest to the left of the complex s-plane, thus improving the damping of these modes. The use of the second objective function results in improving the time domain specifications of the system performance in terms of overshoot and settling time.

Individual design as well as coordinated design of the proposed stabilizers with and without system parameter uncertainties have been investigated and discussed. It has been concluded that the eigenvalue-based objective function can be used to design efficient individual as well as coordinated stabilizers. However, the time-domain-based objective function has the advantage of designing several controllers with different objectives in a coordinated manner. This feature has been utilized to design the UPFC damping stabilizers and internal controllers in a coordinated manner.

In all cases, the damping characteristics of the proposed control schemes to low frequency oscillations over a wide range of operating conditions have been evaluated using the eigenvalue analysis. The effectiveness of the proposed control schemes in enhancing the power system dynamic stability has been verified through comprehensive nonlinear time-domain simulations for a variety of loading conditions. It was clearly shown that the coordinated design approach outperforms the individual designs.

7. Appendix

$M = 8.0$s;	$T'_{do} = 5.044$;	$D = 0.0$;	$x_d = 1.0$;
$x'_d = 0.3$;	$x_q = 0.6$;	$X_T = 0.6$;	$\lvert u_{PSS} \rvert \leq 0.2$ pu;
$K_A = 50$;	$T_A = 0.05$;	$T_w = 5.0$;	$\lvert E_{fd} \rvert \leq 7.3$ pu;
$v = 1.05$ pu;	$x_{tE} = 0.1$;	$x_{BV} = 0.6$;	$K_s = 1.0$;
$T_s = 0.05$;	$x_E = 0.1$;	$x_B = 0.1$;	$C_{dc} = 3$;
$V_{dc} = 2$;			

All resistances and reactances are in pu and time constants are in seconds.

Notes:
1. All simulations using the eigenvalue-based objective function J_e are carried out assuming line 1 open, i.e. $x_T = \infty$.
2. All simulations using the eigenvalue-based objective function J_e are carried out assuming $k_{dp} = -10$ and $k_{di} = 0$.

8. References

Abdel-Magid, Y.L.; Abido, M.A.; Al-Baiyat, S. & Mantawy, A.H. (1999). Simultaneous Stabilization of Multimachine Power Systems via Genetic Algorithms, *IEEE Trans. on Power Sys.*, Vol. 14, No. 4, November 1999, pp. 1428-1439.

Abido, M.A. & Abdel-Magid, Y.L. (1997). Radial basis function network based power system stabilizers for multimachine power systems, *Intl. Conf. Neural Networks*, Vol. 2, 9-12 June 1997, pp. 622 -626

Abido, M.A. (2001). Particle swarm optimization for multimachine power system stabilizer design, *IEEE Power Eng. Society Summer Meeting*, Vol. 3, 15-19 July 2001, pp. 1346 - 1351

Abido, M.A.; Al-Awami, A.T. & Abdel-Magid, Y.L. (2006a). Analysis and design of UPFC damping stabilizers for power system stability enhancement, *IEEE Symposium on Industrial Electronics* ISIE'2006, Vol. 3, July 2006, pp. 2040-2045

Abido, M.A.; Al-Awami, A.T. & Abdel-Magid, Y.L. (2006b). Power system stability enhancement using simultaneous design of damping controllers and internal controllers of a unified power flow controller, the 2006 IEEE *PES General Meeting*, June 2006, pages: 8

Al-Awami, A.T.; Abdel-Magid, Y.L. & Abido, M.A. (2005). Simultaneous stabilization of power systems equipped with unified power flow controller using particle swarm, *The 15th Power Systems Computation Conference*, Session 12, Paper 2, Aug. 2005, pp. 1-7

Al-Awami, A.T.; Abdel-Magid, Y.L. & Abido, M.A. (2006a). Simultaneous stabilization of power system using UPFC-based controllers, *Electric Power Components and Systems*, Vol. 34, No. 9, Sept 2006. pp. 941 – 959

Al-Awami, A.T.; Abdel-Magid, Y.L. & Abido, M.A. (2006b) Power system stability enhancement using unified power flow controllers,' *The 3nd Industrial Electrical and Electronics GCC Conference*, IEEE-GCC3, March 2006

Al-Awami, A.T.; Abdel-Magid, Y.L. & Abido, M.A. (2007). A particle-swarm-based approach of power system stability enhancement with unified power flow controller, *Int'l J. Electrical Power & Energy Syst.*,Vol. 29, 3, March 2007, pp. 251-259

Chen, C.L. & Hsu, Y.Y. (1987). Coordinated synthesis of multimachine power system stabilizer using an efficient decentralized modal control (DMC) algorithm, IEEE *Trans. on Power Systems*, Vol. 9, No. 3, pp. 543-551

Dash, P.K.; Mishra, S. & Panda, G. (2000). A radial basis function neural network controller for UPFC, *IEEE Trans.Power Systems,* Vol. 15, No. 4, Nov. 2000, pp. 1293 -1299

Eberhart, R. & Kennedy J. (1995). A new optimizer using particle swarm theory, *Proc. the Sixth Intl. Symposium on Micro Machine and Human Science*, 4-6 Oct 1995, pp. 39 -43

Gibbard, M.J. (1988). Co-ordinated design of multimachine power system stabilisers based on damping torque concepts, *IEE Proc. Pt. C*, Vol. 135, No. 4, pp. 276-284.

Hamdan, A.M.A. (1999). An investigation of the significance of singular value decomposition in power system dynamics, *Int. Journal Electrical Power and Energy Systems*, 21, pp. 417-424

Heffron, W.G. & Phillips, R.A. (1952). Effect of modern amplidyne voltage regulators on under-excited operation of large turbine generator, *AIEE Trans. Power Apparatus and Systems*, Aug 1952, pp. 692-697.

Huang, Z.; Yinxin, N.; Shen, C.M.; Wu, F.F.; Chen, S. & Zhang, B. (2000). Application of unified power flow controller in interconnected power systems-modeling, interface, control strategy, and case study, *IEEE Trans. Power Systems*, Vol. 15, No. 2 , May 2000, pp. 817 -824

Kennedy, J. & Eberhart, R. (1995). Particle swarm optimization, *Proc. IEEE Intl. Conf. Neural Networks,* 4, Nov/Dec 1995, pp. 1942 –1948.

Klein, M.; Le, L.X.; Rogers, G.J.; Farrokhpay, S. & Balu, N.J. (1995). H∞ damping controller design in large power systems, *IEEE Trans. on Power Systems,* Vol. 10, no. 1, Feb. 1995, pp. 158 -166

Mahran, A.R.; Hogg, B.W. & El-Sayed, M.L. (1992). Co-ordinated control of synchronous generator excitation and static VAR compensator, *IEEE Trans. Energy Conversion*, Vol. 7, Issue 4, Dec. 1992, pp. 615 -622.

Mok, T.K.; Ni, Y. & Wu, F.F. (2000). Design of fuzzy damping controller of UPFC through genetic algorithm, *IEEE Power Eng. Society Summer Meeting*, Vol. 3, 16-20 July 2000, pp. 1889 - 1894

Nabavi-Niaki, A. & Iravani, M.R. (1996). Steady-state and dynamic models of unified power flow controller (UPFC) for power system studies, *IEEE Trans. Power Systems*, Vol. 11, No. 4, Nov. 1996, pp. 1937-1943

Pal, B.C. (2002). Robust damping of interarea oscillations with unified power flow controller, *IEE Proc. Gen. Trans. and Distrib.*, Vol. 149, No. 6, pp. 733-738.

Samarasinghe, V.G.D.C. & Pahalawaththa, N.C. (1997). Damping of multimodal oscillations in power systems using variable structure control techniques, *IEE Proc. Gen. Trans. and Distrib.*, Vol. 144, No. 3, pp. 323-331.

Seo, J.C.; Moon, S.; Park, J.K. & Choe, J.W. (2001). Design of a robust UPFC controller for enhancing the small signal stability in the multi-machine power systems, I*EEE Power Eng. Society Winter Meeting*, Vol. 3 , 28 Jan.-1 Feb. 2001, pp. 1197 -1202

Shi, Y. & Eberhart, R. (1998). A modified particle swarm optimizer, *The 1998 IEEE Intl. Conf. on Evolutionary Computation Proc.*, IEEE World Congress on Computational Intelligence., 4-9 May 1998, pp. 69 – 73.

Vilathgamuwa, M.; Zhu, X. & Choi, S.S. (2000). A robust control method to improve the performance of a unified power flow controller, *Electric Power System Research*, 55, pp. 103-111.

Wang, H.F. (1999a). Damping function of unified power flow controller, *IEE Proc. Gen. Trans. and Distrib.*, Vol. 146, No. 1, pp. 81-87.

Wang, H.F. (1999b). Application of modeling UPFC into multi-machine power systems, *IEE Proc. Gen. Trans. and Distrib.*, Vol. 146, No. 3, pp. 306-312.
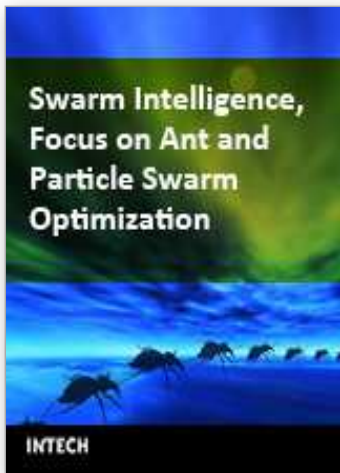
Swarm Intelligence, Focus on Ant and Particle Swarm Optimization

Edited by FelixT.S.Chan and Manoj KumarTiwari

In the era globalisation the emerging technologies are governing engineering industries to a multifaceted state. The escalating complexity has demanded researchers to find the possible ways of easing the solution of the problems. This has motivated the researchers to grasp ideas from the nature and implant it in the engineering sciences. This way of thinking led to emergence of many biologically inspired algorithms that have proven to be efficient in handling the computationally complex problems with competence such as Genetic Algorithm (GA), Ant Colony Optimization (ACO), Particle Swarm Optimization (PSO), etc. Motivated by the capability of the biologically inspired algorithms the present book on "Swarm Intelligence: Focus on Ant and Particle Swarm Optimization" aims to present recent developments and applications concerning optimization with swarm intelligence techniques. The papers selected for this book comprise a cross-section of topics that reflect a variety of perspectives and disciplinary backgrounds. In addition to the introduction of new concepts of swarm intelligence, this book also presented some selected representative case studies covering power plant maintenance scheduling; geotechnical engineering; design and machining tolerances; layout problems; manufacturing process plan; job-shop scheduling; structural design; environmental dispatching problems; wireless communication; water distribution systems; multi-plant supply chain; fault diagnosis of airplane engines; and process scheduling. I believe these 27 chapters presented in this book adequately reflect these topics.

How to reference

In order to correctly reference this scholarly work, feel free to copy and paste the following:

INTECH

open science | open minds